

This article was downloaded by: [University Of Maryland]

On: 26 November 2013, At: 09:22

Publisher: Taylor & Francis

Informa Ltd Registered in England and Wales Registered Number: 1072954 Registered office: Mortimer House, 37-41 Mortimer Street, London W1T 3JH, UK



Aerosol Science and Technology

Publication details, including instructions for authors and subscription information:
<http://www.tandfonline.com/loi/uast20>

Development of a Pulsed-Field Differential Mobility Analyzer: A Method for Measuring Shape Parameters for Nonspherical Particles

Mingdong Li ^{a b}, Rian You ^{a b}, George W. Mulholland ^{a b} & Michael R. Zachariah ^{a b}

^a Department of Chemical and Biomolecular Engineering , University of Maryland , College Park , Maryland , USA

^b Department of Chemistry and Biochemistry , National Institute of Standards and Technology , Gaithersburg , Maryland , USA

Accepted author version posted online: 03 Oct 2013.Published online: 03 Oct 2013.

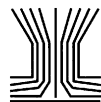
To cite this article: Mingdong Li , Rian You , George W. Mulholland & Michael R. Zachariah (2014) Development of a Pulsed-Field Differential Mobility Analyzer: A Method for Measuring Shape Parameters for Nonspherical Particles, *Aerosol Science and Technology*, 48:1, 22-30, DOI: [10.1080/02786826.2013.850150](https://doi.org/10.1080/02786826.2013.850150)

To link to this article: <http://dx.doi.org/10.1080/02786826.2013.850150>

PLEASE SCROLL DOWN FOR ARTICLE

Taylor & Francis makes every effort to ensure the accuracy of all the information (the "Content") contained in the publications on our platform. However, Taylor & Francis, our agents, and our licensors make no representations or warranties whatsoever as to the accuracy, completeness, or suitability for any purpose of the Content. Any opinions and views expressed in this publication are the opinions and views of the authors, and are not the views of or endorsed by Taylor & Francis. The accuracy of the Content should not be relied upon and should be independently verified with primary sources of information. Taylor and Francis shall not be liable for any losses, actions, claims, proceedings, demands, costs, expenses, damages, and other liabilities whatsoever or howsoever caused arising directly or indirectly in connection with, in relation to or arising out of the use of the Content.

This article may be used for research, teaching, and private study purposes. Any substantial or systematic reproduction, redistribution, reselling, loan, sub-licensing, systematic supply, or distribution in any form to anyone is expressly forbidden. Terms & Conditions of access and use can be found at <http://www.tandfonline.com/page/terms-and-conditions>



Development of a Pulsed-Field Differential Mobility Analyzer: A Method for Measuring Shape Parameters for Nonspherical Particles

Mingdong Li,^{1,2} Rian You,^{1,2} George W. Mulholland,^{1,2} and Michael R. Zachariah^{1,2}

¹Department of Chemical and Biomolecular Engineering, University of Maryland, College Park, Maryland, USA

²Department of Chemistry and Biochemistry, National Institute of Standards and Technology, Gaithersburg, Maryland, USA

For a nonspherical particle, a standard differential mobility analyzer (DMA) measurement yields a mobility-equivalent spherical diameter, but provides no information about the degree of sphericity. However, given that the electrical mobility for nonspheres is orientation-dependent, and that orientation can be manipulated using electric fields of varying strength, one can, in principle, extract some type of shape information through a systematic measurement of mobility as a function of particle orientation. Here, we describe the development of a pulsed-field differential mobility analyzer (PFDMA) which enables one to change the peak E -field experienced by the particle to induce orientation, while still maintaining the same time-averaged field strength as a standard DMA experiment. The instrument is validated with polystyrene latex (PSL) spheres with accurately known size, and gold rods with dimensions accurately determined by transmission electron microscopy (TEM). We demonstrate how the instrument can be used for particle separation and extraction of shape information. In particular, we show how one can extract both length and diameter information for rod-like particles. This generic approach can be used to obtain dynamic shape factors or other multivariate dimensional information (e.g., length and diameter).

1. INTRODUCTION

Nanomaterials are widely applied and studied in medicine, electronics, biomaterials, and environmental science. Effective measurement and accurate characterization of nanomaterials play a critical role in the development of nanotechnology. It

is well known that many of the properties of particles are size-dependent. Moreover, for aspherical structures such as nanorods and nanowires, the properties are also greatly influenced by their shapes. For example, gold nanorods are useful for the formation of many functional composite materials due to their special light scattering and absorption properties (Ni et al. 2008; Alkilany et al. 2012). Nonspherical particles also have important effects on environment and human health. Soot aggregates produced by combustion are highly nonspherical ramified structures with noninteger fractal dimensions. The common feature of all these materials is that they are nonspherical and thus cannot be dimensionally characterized by just one length scale. To obtain size and shape information of nanoparticles, microscopy techniques, such as transmission or scanning electron microscopy (TEM/SEM), are traditionally applied. However, in these off-line methods, good sampling methods and time-consuming operations are needed for a precise distribution measurement. It is also reported that the sampling and imaging process itself may cause coalescence of small clusters (Schmid and Chi 1998). The differential mobility analyzer (DMA) is the gold-standard measurement method for obtaining a complete electrical-mobility-size distribution of nanoparticles in the aerosol phase (Flagan 2008). For a spherical particle, the electrical mobility diameter is equivalent to its geometric diameter. However, if the particle is nonspherical, the resulting electrical mobility diameter is that diameter for a sphere with the same mobility as the analyte particle. For example, Song et al. (2005) investigated the relationship between the electrical mobility size and particle shape, by changing the particle shape from nanorod to sphere by heating the particles from 25°C to 800°C, and showed that the mobility diameters decreased from 55 nm to 25 nm. Since the mobility size measured in the DMA depends on the drag force on the particles, thus for a nonspherical particle, mobility necessarily depends on orientation with respect to the applied electric field (Kousaka et al. 1996; Kim et al. 2007; Zelenyuk and Imre 2007; Li et al. 2012, 2013). In principle then, an orientation-dependent

Received 4 June 2013; accepted 22 September 2013.

Disclaimer: Reference to commercial equipment or supplies does not imply endorsement by the University of Maryland or the National Institute of Standards and Technology.

Address correspondence to Michael R. Zachariah, Department of Chemical and Biomolecular Engineering, University of Maryland, 2125 Martin Hall, College Park, MD 20742, USA. E-mail: mrz@umd.edu

mobility measurement should yield some information on particle shape.

Kousaka et al. (1996) measured the dynamic shape factor for doublets of uniform spheres (polystyrene latex particles; PSL) in the transition regime and pointed out that the orientation of doublets is a function of electric field in the DMA and the size of doublets. Zelenyuk and Imre (2007) applied this idea to more aspherical particles and showed that the dependence of electrical mobility size on electric field can be applied to separate particles based on their shape. Kim et al. (2007) measured the length of carbon nanotubes considering a scalar expression of drag force.

However, none of these studies provide a rigorous expression, which can present the appropriate relationship between the measured electrical mobility size (or detection voltage) and the geometric shape of particles. In the studies of Li et al. (2012, 2013), we developed an orientation-averaged electrical mobility theory for rigid axisymmetric particles undergoing Brownian motion by considering the electrical polarization of the particles in an electric field. This theory was validated by experimental results of well-defined doublets of NIST traceable size standard PSL spheres (127 nm, 150 nm, 200 nm, and 240 nm) (Li 2012) and monodisperse gold rods (Li et al. 2013). This model (which requires information on the friction coefficient tensor) has been further extended to any particle shape in a systematic study of the mobility of nonspherical particles (Li 2012). The particle geometric shape information can then be extracted from experimental mobility measurements at various electric fields by fitting Li's theory (Li et al. 2013).

To obtain the shape information by measuring the electrical mobility under different electric fields, a new instrument, a pulsed differential mobility analyzer (PFDMA), is implemented. Pulsed electric fields have been previously used for measuring the light scattering by aligned and randomly oriented agglomerate particles (Cheng et al. 1991; Weiss et al. 1992; Colbeck et al. 1997); however, this is the first application for the electric mobility of a particle. This new method enables one to change the peak E-field experienced by the particle, while still maintaining the same time-averaged field. In so doing, one could, in principle, systematically change the average orientation of a nonspherical particle and thus its mobility without varying the flow rates in the measurement setup. The instrument is tested on PSL spheres and gold nanorods with known size and shape (conducting monodisperse nonspheres), and the result shows that the PFDMA can be used for particle separation and particle shape information measurements. Long slender gold nanorods were chosen because the cylindrical shape is one of the few nonspherical shapes where there is an exact solution in the free molecular limit and because the shape affect is most pronounced for a shape with a large aspect ratio. Another key experimental factor was the monodispersity of the rods in terms of diameter and length. A final important feature is the high conductivity of the gold nanorod.

2. THEORETICAL MODELS FOR SHAPE MEASUREMENT

The particle electrical mobility, Z_p , is defined by: $Z_p = v_r / E$, where v_r is the particle drift velocity and E is the magnitude of the electric field. By equating the electrostatic attraction force to the drag force on a spherical particle, electrical mobility, Z_p can be obtained as

$$Z_p = \frac{neC_c(d_m)}{3\pi\eta d_m}, \quad [1]$$

where n is the number of elementary charges on the particle, d_m the electrical mobility diameter, and $C_c(d_m)$ the Cunningham slip correction factor, which was parameterized by Allen and Raabe (1985). The electrical mobility diameter d_m of a sphere is equal to its geometric diameter, and the electrical mobility Z_p is only a function of this spherical diameter based on Equation (1) and independent of electric field in the DMA. However, for a nonspherical particle, d_m is the equivalent diameter of a sphere having the same drag force, and the size and shape information of this nonspherical particle is contained in the electrical mobility, Z_p . Unlike a spherical particle for which the electrical mobility is independent of field strength, the nonspherical particle, because of its field-dependent orientation, has a field-dependent mobility Z_p (Shape, E).

For nonspherical particles, Equation (1) can be used to get an equivalent spherical diameter, but is not sufficient to obtain the geometric shape information. Li et al. (2012) presented a general form for the orientation-averaged mobility for an axisymmetric particle in an electric field which has been validated by experimental results of doublets with primary particle size larger than 125 nm (Li 2012) and gold nanorods (Li et al. 2013), i.e.,

$$\overline{Z_p} = q[K_{\perp}^{-1} + (K_{\parallel}^{-1} - K_{\perp}^{-1})\langle\cos^2\theta\rangle], \quad [2]$$

where q is the net charge on the particle, K_{\perp} is the principal component of the friction coefficient tensor perpendicular to the axial direction, K_{\parallel} is the component parallel to the axial direction, $\langle\cos^2\theta\rangle = \int_0^\pi \cos^2\theta f(\theta) \sin\theta d\theta$, is the orientationally averaged $\cos^2(\theta)$, which is a function of the electric field strength which leads to the E dependence of the average mobility, and $f(\theta)$ is the orientational probability function with $\int_0^\pi f(\theta) \sin\theta d\theta = 1$. The evaluation of Equation (2) requires a knowledge of K_{\perp} and K_{\parallel} , which depend on the drag model ($F_{\text{drag}} = -\hat{K} \cdot \vec{V}_d$) specific to the geometry of interest (e.g., ellipsoid, rod, and doublets of spheres) and the orientation average value $\langle\cos^2\theta\rangle$. The detailed calculations of K_{\perp} and K_{\parallel} for nanorods and ellipsoids in the three regimes, and the calculations of $\langle\cos^2\theta\rangle$ were shown in Li et al. (2012). Combining the orientation-averaged mobility expression and the experimental measured mobility, one can obtain particle shape information.

2.1. Orientation-Averaged-Mobility for a Slender Conducting Rod in the Free Molecular Regime

The friction coefficients, K_{\parallel} and K_{\perp} , in Equation (2) are given by Equations (A1) and (A2) in Li et al. (2012) for a rod (length L_r , diameter d_r , aspect ratio $\beta = L_r/d_r$) in the free molecular regime (where the gas viscosity, $\eta = 1.8325 \times 10^{-5}$ kg m⁻¹ s⁻¹; the mean free path of gas, $\lambda = 67.3$ nm; and the momentum accommodation, $f = 0.9$ used in this work [Dahneke 1973])

$$K_{\parallel} = \frac{\pi \eta d_r^2}{2\lambda} \left[\left(\beta + \frac{\pi}{4} - 1 \right) f + 2 \right], \quad [3a]$$

$$K_{\perp} = \frac{\pi \eta d_r^2}{2\lambda} \left[\left(\frac{\pi}{4} - 2 \right) \beta + \frac{1}{2} \right] f + 2\beta, \quad [3b]$$

and $\langle \cos^2 \theta \rangle$ given by Equation (22) of Li et al. (2012), for a conducting rod using the induced dipole polarization energy

$$\langle \cos^2 \theta \rangle = \frac{1}{2\delta} \left[\frac{2\sqrt{\delta} e^{\delta}}{\sqrt{\pi} \operatorname{Erfi}(\sqrt{\delta})} - 1 \right], \quad [4]$$

where

$$\delta = \frac{(\alpha_{\parallel} - \alpha_{\perp}) E^2}{2kT},$$

α_{\parallel} and α_{\perp} are the two principal components of polarizability, E is the intensity of electric field, k is the Boltzmann constant, $T = 296.15$ K used in this work, and $\operatorname{Erfi}(z) = \frac{2}{\sqrt{\pi}} \int_0^z e^{t^2} dt$ is the imaginary error function.

Evaluation of the mobility expression (Equation (2)) is mathematically simplified by making a slender conducting rod approximation (length L_r , diameter d_r , and aspect ratio $\beta = L_r/d_r \gg 1$) for the values of polarizability (α_{\parallel} and α_{\perp}) in Equation (4) (Li et al. 2013)

$$\alpha_{\parallel} = \frac{\varepsilon_0 \pi d_r^3 \beta^3}{4[\ln(2\beta) - 1]}, \quad \alpha_{\perp} = \frac{\varepsilon_0 \pi d_r^3 \beta}{2}, \quad [5]$$

where ε_0 is the free-space permittivity. The deviation of δ for $\beta = 16$ between the value given by the slender approximation (5) and given by the full theory (Li et al. 2012, Equations (A13) and (A14)) is about 0.66%.

At low field strengths, the thermal energy dominates the aligning energy, and Brownian dynamics results in a random orientation. As the electric field increases, the slender rod will tend to align and result in a larger electric mobility. In Figure 1, we plot the normalized (relative to random orientation) electrical mobility vs. applied electric field of a slender conducting rod (calculated in free molecular regime with Equations (2)–(5)) (Li et al. 2012, 2013) for a wide range of aspect ratios, β , and with diameter $d_r = 15$ nm. A clear increase in mobility is observed with increasing field strength for all aspect ratios. The onset

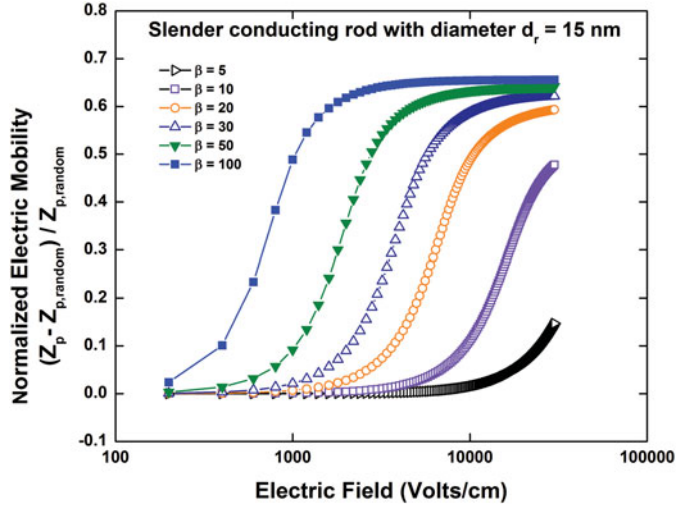


FIG. 1. Theoretical calculation of the effect of electric field on the scaled mobility (relative to the mobility for a randomly oriented rod) for various aspect ratio slender conducting rod with rod diameter $d_r = 15$ nm. Mobility is calculated in the free molecular regime using Dahneke's expression (3a)–(3b). The air breakdown limit is 30,000 V/cm. (Color figure available online.)

of alignment occurs at lower field strength with increasing β . The sigmoidal shape of the curves is key to being able to size nanowires and separate them from spheres.

We will demonstrate in Section 5 that least-squares fitting is mathematically efficient in extracting both the diameter and the length of gold rods from the experimental mobility measurements in various electric fields using Equations (2)–(5).

3. PULSED-FIELD DIFFERENTIAL MOBILITY ANALYZER (PFDMA)

The shape information for a nonspherical particle is contained in the electrical mobility as shown in Equation (2), which is usually a nonlinear function of electric field and particle shape. Once the mobility is measured from a DMA at various electric field magnitudes, one can fit Equation (2) to extract the particle shape information.

One way of measuring the effect of particle alignment under different electric fields is to vary the sheath flow in the DMA. However, changing flow is not very convenient, and in so doing the instrument resolution is also changed. In this section, we introduce a new instrumental technique, employing a Pulsed DMA, which allows one to change the electric field acting on the nonspherical particle by only changing the duty cycle of a pulsed electric field in a DMA rather than changing the flow. Furthermore, this approach also allows one to employ very high fields, to induce orientation increasing mobility, while keeping the average field moderate through changes in the duty cycle.

Consider a square-wave pulse going from zero to $-V$ with a duty cycle equal to a fraction of the period. As illustrated in Figure 2, while the particle is exposed to the high field, it will

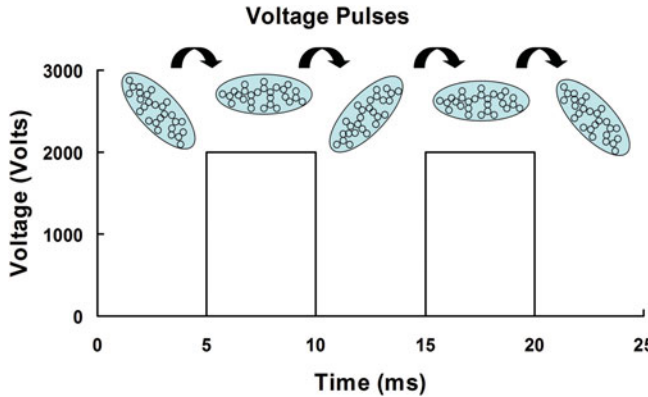


FIG. 2. Oscillating electric field to align particles (wires or aggregates). In this example, the pulse frequency is 100 Hz, the duty cycle is 50%, with a 2000 V pulse. Thus, the average voltage is 1000 V. (Color figure available online.)

be partially aligned, and then returns to a random orientation when the field is removed. After removal of the field, there is no radial movement of the particle in the DMA, so the effective movement in the radial direction only takes place when the particle is exposed to the high field. The change in the electrical mobility is measured as the alignment field intensity is changed.

A key concept is that for a spherical particle the precipitation time from the inlet to the exit slit is only a function of the time-averaged potential. Thus, if 1000 volts with a DMA sheath flow rate, Q_{sh} , corresponds to particles exiting the DMA at the peak in the inlet mobility distribution for spherical particles, then a pulsed field with a 25% duty cycle and a 4000 V at the DMA sheath flow rate, Q_{sh} , will also result in the peak mobility exiting the DMA. Figure 3 shows how one can vary the pulse field by about a factor of 2 or 4 while still keeping the average field constant. On the other hand, a nonspherical particle passing through the DMA will be partially aligned by the field so that the peak mobility will be shifted as the pulse width is decreased. During the period of alignment under high field,

which is the effective time for particles traveling along the radial direction, its drag will be lower and thus its mobility higher than the equivalent sphere having mobility equal to that of the nonspherical particle uniformly averaged over all orientations. If the effect of the rise time of the pulse on the electrical mobility is negligible (see discussion in the next section), the pulsed field with a 25% duty cycle at sheath flow, Q_{sh} , is equivalent to a DC field at sheath flow, $4 \times Q_{sh}$. Thus, the mobility measured by a PFDMA is given by

$$Z_p = \frac{(Q_{sh}/D_{cycle}) \ln(r_{out}/r_{in})}{2\pi V_e L_d}, \quad [6]$$

where r_{in} is the radius of the inner electrode of DMA, r_{out} is the radius of the outer electrode of DMA, L_d is the “active” length of DMA electrode, Q_{sh} is the sheath flow rate, D_{cycle} is the duty cycle of the pulse, and V_e is the DMA voltage. Theoretically, the transfer function and resolution of the PFDMA are the same as the DMA used in the PFDMA system. The ability to distinguish a rod, however, is determined by the extent to which the rod can be aligned, which is dependent on the field and aspect ratio.

In this work, the PFDMA is experimentally validated by comparing its measured results with the DMA (under DC voltage) with corresponding sheath flow rates. The instrument is tested with PSL spheres with precisely known size, and gold rods, with dimensions determined by TEM. We show how both length and diameter of rods can be determined from the PFDMA measurements.

4. EXPERIMENTAL AND RESULTS

4.1. Pulser System for PFDMA

To produce a square-wave pulsed field requires a function generator (gate signal source), a pulse generator, and a high-voltage DC power supply. The pulse generator converts the input DC voltage to a square wave of prescribed frequency and pulse width from the signal generator as shown in Figure 4. The critical component is the pulse generator (DEI, PVX-4110) which provides the need for a rapid rise time, adjustable pulse width, and a clean square high voltage wave. A key constraint for high-voltage high-frequency output is that the output capacitance be less than about 200 pF. The performance of the pulse generator with the DMA attached was verified by monitoring the output of the pulse generator using an oscilloscope. The generated pulse had at most a 60 ns rise and fall time, and an adjustable pulse width from 200 ns to DC. Consider that for a test rod-like particle, one similar to that to be evaluated later in this work (diameter = 17 nm and length \sim 250 nm), the rotational relaxation time is about $\sim 10^{-5}$ s in the free molecular regime (Li et al. 2014). Thus, both the rise time of the electronics and the particle rotational relaxation time are small compared to the pulse width (250 ms > width > 0.5 ms for the long DMA and 50 ms > width > 0.5 ms for the nano-DMA). The pulse widths applied in this work are short relative to the transit time

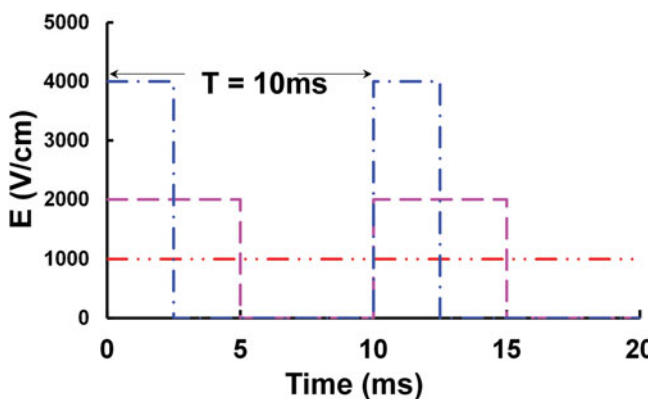


FIG. 3. Illustration of the relationship between the electric field and the pulse width to maintain a constant average field. Duty cycles vary from 100%, 50%, to 25% with pulse frequency 100 Hz, and the corresponding fields are 1000, 2000, and 4000 V/cm, respectively. (Color figure available online.)

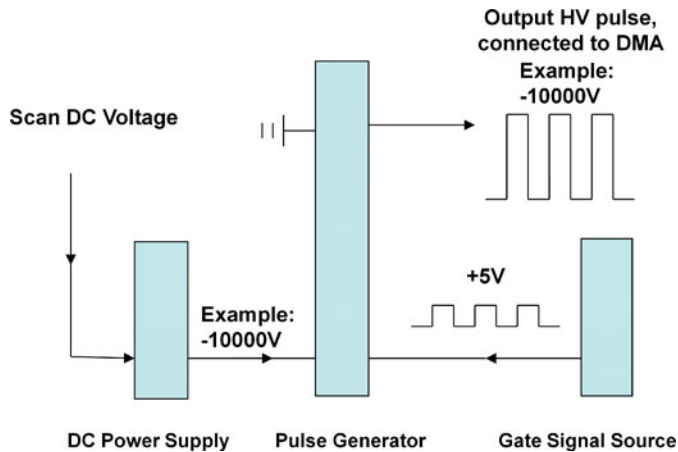


FIG. 4. Schematic of pulser system for generating square-wave high-voltage pulses. (Color figure available online.)

through the DMA (~ 860 ms for nano-DMA and ~ 8.3 s for long DMA).

4.2. PFDMA Evaluation

The PFDMA was first evaluated using a mixture of two spherical singlet NIST traceable-size PSL particles, of 127.1 nm (Thermo Scientific 3125A) and 200 nm (Thermo Scientific 3200A) to test the mobility distribution of two spherical particles at various frequencies. Next, we evaluated the PFDMA using colloidal gold nanorods (Nanopartz Inc.; MUTAB-coated conjugated gold nanorods; 10 nm, SPR = 2000 nm, 0.25 mg, 1 mL; C12N-10-2000-TMU-0.25) to test the mobility of nonspherical particles, at various frequencies.

- Validation of PFDMA using spherical particles

The PFDMA system is validated by measuring the mobility sizes of spherical particles, and comparing them with the results from a standard DMA.

Spherical PSL particles (PSL 127.1 nm and 200 nm spheres mixed in one sample) were aerosolized using a constant output pressure atomizer (TSI Inc., Model 3076), and dried with two diffusion dryers before entering a neutralizer, which provides a bipolar charge distribution to the particles. The neutralized particles then pass through a long DMA (TSI Inc., Model 3081) at DC voltage or a PFDMA for particle mobility size measurement and counted with an ultrafine condensed particle counter (CPC) (TSI Inc., Model 3025A). The PFDMA is a standard long differential mobility analyzer column (TSI Inc., Model 3081) connected to high-voltage pulses generated with a pulser system described in Figure 4. All ratios of the sheath to aerosol flow exceeded 20 to guarantee suitably high size resolution. To avoid the effects of time-varying electric field as the particles go through the DMA, we operated the DMA in the step mode, and kept the step suffi-

ciently long to ensure a complete transit through the DMA system before the voltage was changed (up to 45 s).

The DMA was calibrated by measuring the mobility of 100.7 nm NIST standard reference material (SRM) particles and then adjusting the value of the flow in Equation (6) so that the measured mobility is equal to the mobility of a 100.7 nm SRM particle.

The mobility sizes of PSL 127.1 nm and 200 nm spheres were measured at DC voltages using a standard long DMA at sheath flow rates $Q_{sh} = 3$ l/min (0.5×10^{-4} m³/s) and $Q_{sh} = 12$ l/min (2×10^{-4} m³/s). The same sample was also measured in a PFDMA with flow rates $Q_{sh} = 3$ l/min (0.5×10^{-4} m³/s) and duty cycle = 25% (where $Q_{sh}/D_{cycle} = 12$ l/min) at 1 Hz, 2 Hz, 5 Hz, 10 Hz, 50 Hz, 200 Hz, and 500 Hz. The mobility size of this 127.1 nm PSL sphere was calibrated by 100.7 nm NIST standard reference material (PSL sphere) in a separate experiment. Then, the sheath flows were calibrated in all experiments by using the singlet peaks of 127.1 nm, i.e., obtaining the sheath flow rates and duty cycles by making the first singlet peaks showing exactly as 127.1 nm. Once the sheath flow of 3 l/min was calibrated, it was then fixed for all PFDMA measurements. The duty cycles were then calibrated in the PFDMA measurement by using the singlet peaks of 127.1 nm. Using this calibration, the mobility sizes of the second singlet peaks (200 nm PSL) are shown in Figure 5. The results show that so long as the average field is held constant the variation of the pulse frequency does, in fact, lead to a constant mobility for spheres as expected and validates that the applied fields within the DMA are as expected. This is the expected result because the aerosol relaxation time is 10^{-7} s, which is a factor of 10^4 less than the pulse time.

- Validation of PFDMA using gold nanorods

Next, we turn to nonspheres where alignment effects are expected, and we compare the PFDMA with a standard DMA. Gold nanorods, whose dimensions were determined by TEM experiments, diameter 17.1 nm and length 263 nm (with 4% uncertainty), were used for validating the performance of the PFDMA method for a nonsphere. The colloidal gold nanorod solution (Nanopartz Inc.; MUTAB-coated conjugated gold nanorods; 10 nm, SPR = 2000 nm, 0.25 mg, 1 mL; C12N-10-2000-TMU-0.25) was aerosolized using a 40-μm inner diameter capillary mounted in an electrospray aerosol generator (TSI Inc., Model 3480) with a neutralizer to provide a bipolar charge distribution to the particles. The neutralized particles were then passed through a nano-DMA (TSI Inc., Model 3085) and a PFDMA for particle mobility selection and counted with an ultrafine CPC (TSI Inc.,

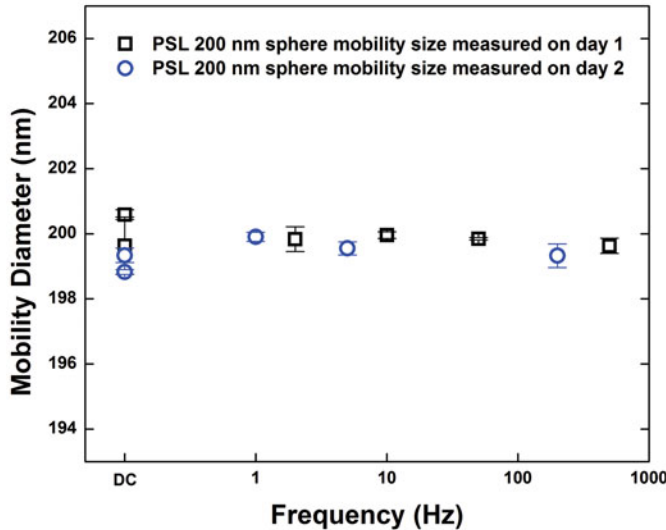


FIG. 5. Mobility diameter of 200 nm spheres. Measured at DC voltages using a standard long DMA at sheath flow rates $Q_{sh} = 3 \text{ l/min}$ ($0.5 \times 10^{-4} \text{ m}^3/\text{s}$) and $Q_{sh} = 12 \text{ l/min}$ ($2 \times 10^{-4} \text{ m}^3/\text{s}$). The same sample was also measured in a PFDMA with flow rates $Q_{sh} = 3 \text{ l/min}$ ($0.5 \times 10^{-4} \text{ m}^3/\text{s}$) and duty cycle = 25% at 1 Hz, 2 Hz, 5 Hz, 10 Hz, 50 Hz, 200 Hz, and 500 Hz. The uncertainty bars were based on three repeat measurements. (Color figure available online.)

Model 3025A). More details on the DMA measurement method can be found in Li et al. (2011a, 2011b) and Guha et al. (2012). The PFDMA here is a standard nanodifferential mobility analyzer column (TSI Inc., Model 3085) connected to high-voltage pulses generated with a pulser system described in Figure 4.

The mobility size of the gold nanorods was measured under DC voltages (standard nano-DMA) at 3 l/min ($0.5 \times 10^{-4} \text{ m}^3/\text{s}$), 6 l/min ($1 \times 10^{-4} \text{ m}^3/\text{s}$), and 12 l/min ($2 \times 10^{-4} \text{ m}^3/\text{s}$) sheath flow rates, respectively; and under pulsed voltages (PFDMA) at 3 l/min ($0.5 \times 10^{-4} \text{ m}^3/\text{s}$) sheath flow rate with a pulse duty cycle of 25% and 50% and frequencies of 5 Hz, 10 Hz, 100 Hz, and 500 Hz, and at 6 l/min ($1 \times 10^{-4} \text{ m}^3/\text{s}$) sheath flow rate with a pulse duty cycle of 50% and frequencies of 5 Hz, 10 Hz, 100 Hz, and 500 Hz, respectively. The experimental conditions of low, intermediate, and high electric fields are shown in Table 1. All ratios of the sheath to aerosol flow exceeded 20 to guarantee suitably high size resolution. To avoid the effects of time-varying electric field as the particles go through the DMA, we operated the DMA in the step mode, and kept the step sufficiently long to ensure a complete transit through the DMA system before the voltage was changed.

The mobility sizes of the gold nanorods were calibrated with 60 nm PSL spheres under the same experimental conditions. The mobility size of these 60 nm PSL spheres was calibrated by 100.7 nm NIST standard reference material (PSL sphere) in a separate mea-

surement. The measurements with the standard reference material (100.7 nm), 60 nm PSL sphere, and the gold nanorod were repeated three times, respectively, and the assignment of DMA detection voltage was obtained by averaging the three means of the Gaussian fits to the experimental profile. The calibration procedures for gold rods using 60 nm PSL are as follows. The exact sheath flow value was assigned by measurement of the 60 nm PSL sphere at the same condition as the gold nanorod measurement under DC voltage. Once the sheath flow was calibrated, it was then fixed for all successive PFDMA measurements. The duty cycle was then calibrated in the PFDMA measurement using the 60 nm PSL. Using this calibrated sheath flow value and the duty cycle, the mobility sizes of the gold rod could be determined by Equation (6). Uncertainty bars for mobility sizes are based on three repeat voltage scans.

In Figure 6, we show the mobility size shift of gold nanorods measured by the PFDMA, a standard DMA in high ($Q_{sh}/D_{cycle} = 12 \text{ l/min}$) and intermediate electric fields ($Q_{sh}/D_{cycle} = 6 \text{ l/min}$). The results are presented as a mobility shift (on Y-axis) as relative to the low electric field (DC voltage, 3 l/min) case ($d_m \sim 73 \text{ nm}$) as a function of pulse frequency. The detailed experimental conditions are shown in Table 1.

First, the measured mobility sizes for gold nanorods (non-spherical particle) are consistent between a standard DMA

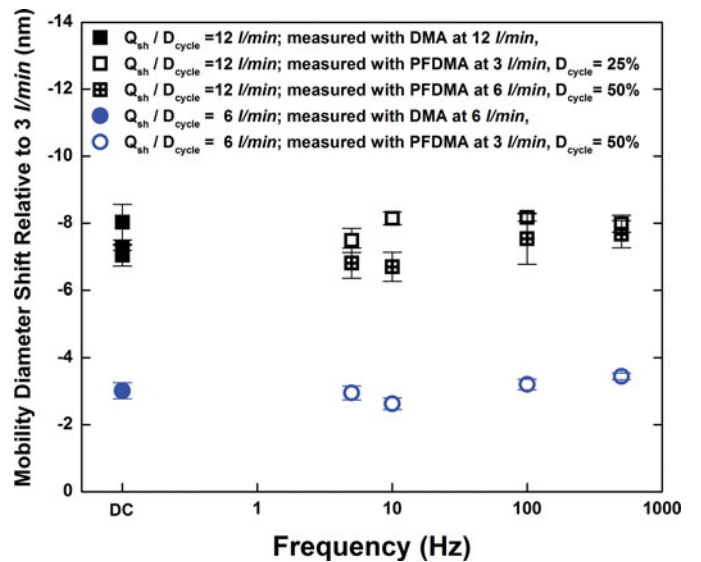


FIG. 6. Mobility size shift of gold nanorod ($17 \text{ nm} \times 270 \text{ nm}$) with respect to the low DC voltage 3 l/min ($0.5 \times 10^{-4} \text{ m}^3/\text{s}$) case ($d_m \sim 73 \text{ nm}$) versus pulse frequency. The zero frequency condition is the DC voltage case. The mobility sizes measured between a standard DC voltage nano-DMA and a PFDMA with the same flow rate to duty cycle ratio are consistent among all experiments. There is no apparent frequency dependency among all measured frequencies. The uncertainty bars were based on three repeat measurements. (Color figure available online.)

TABLE 1
Experimental conditions for gold nanorod mobility measurements

Low electric field ($Q_{sh}/D_{cycle} = 3 \text{ l/min}$)	DC voltage; $Q_{sh} = 3 \text{ l/min}$ ($Q_a = 0.07 \text{ l/min}$)
Intermediate electric field ($Q_{sh}/D_{cycle} = 6 \text{ l/min}$)	DC voltage; $Q_{sh} = 6 \text{ l/min}$ ($Q_a = 0.15 \text{ l/min}$)
High electric field ($Q_{sh}/D_{cycle} = 12 \text{ l/min}$)	Pulsed voltage with duty cycle = 50%; $Q_{sh} = 3 \text{ l/min}$ ($Q_a = 0.07 \text{ l/min}$); 5 Hz Pulsed voltage with duty cycle = 50%; $Q_{sh} = 3 \text{ l/min}$ ($Q_a = 0.07 \text{ l/min}$); 10 Hz Pulsed voltage with duty cycle = 50%; $Q_{sh} = 3 \text{ l/min}$ ($Q_a = 0.07 \text{ l/min}$); 100 Hz Pulsed voltage with duty cycle = 50%; $Q_{sh} = 3 \text{ l/min}$ ($Q_a = 0.07 \text{ l/min}$); 500 Hz DC voltage; $Q_{sh} = 12 \text{ l/min}$ ($Q_a = 0.3 \text{ l/min}$) Pulsed voltage with duty cycle = 50%; $Q_{sh} = 6 \text{ l/min}$ ($Q_a = 0.15 \text{ l/min}$); 5 Hz Pulsed voltage with duty cycle = 50%; $Q_{sh} = 6 \text{ l/min}$ ($Q_a = 0.15 \text{ l/min}$); 10 Hz Pulsed voltage with duty cycle = 50%; $Q_{sh} = 6 \text{ l/min}$ ($Q_a = 0.15 \text{ l/min}$); 100 Hz Pulsed voltage with duty cycle = 50%; $Q_{sh} = 6 \text{ l/min}$ ($Q_a = 0.15 \text{ l/min}$); 500 Hz Pulsed voltage with duty cycle = 25%; $Q_{sh} = 3 \text{ l/min}$ ($Q_a = 0.07 \text{ l/min}$); 5 Hz Pulsed voltage with duty cycle = 25%; $Q_{sh} = 3 \text{ l/min}$ ($Q_a = 0.07 \text{ l/min}$); 10 Hz Pulsed voltage with duty cycle = 25%; $Q_{sh} = 3 \text{ l/min}$ ($Q_a = 0.07 \text{ l/min}$); 100 Hz Pulsed voltage with duty cycle = 25%; $Q_{sh} = 3 \text{ l/min}$ ($Q_a = 0.07 \text{ l/min}$); 500 Hz

and the PFDMA with the same flow rate to duty cycle ratio (Q_{sh}/D_{cycle}) which defines the intensity of the electric field. The mobility size shift, is $\sim 8 \text{ nm}$, at high ($Q_{sh}/D_{cycle} = 12 \text{ l/min}$) and $\sim 3 \text{ nm}$, at intermediate field ($Q_{sh}/D_{cycle} = 6 \text{ l/min}$) for both PFDMA and standard DMA measurements, with no discernible frequency dependency with this normalization.

These results clearly show that the PFDMA when used on both spherical and rod-like particles behaves as expected. The PFDMA enables one to change the peak E -field experienced by the particle without changing the flow, and hence can be used to measure the mobility of a nonspherical particle at various electric fields which opens up the opportunity to an eventual shape evaluation as will be discussed in the next section.

4.3. Extracting Particle Geometric Shape Information from Pulsed Mobility Measurements

In this section, we demonstrate a least-squares fitting procedure that can be employed to extract the dimensions (diameter and length) of gold nanorods by measuring the mobility shift at various peak electric fields and the use of the model equations (2)–(5).

Figure 7 shows the experimentally determined mobility of gold rods using the PFDMA as a function of average applied field. In this analysis, we regard mobility as a constant corresponding to an electric field equal to the electrode voltage divided by the radial distance between the two electrodes. Our calculation shows that the radial variation in the electric field affects the value of the mobility by less than 0.7%. The mobility at three high electric fields were measured by a PFDMA with nanocolumn, and the mobility at two low electric fields were measured with a long-column PFDMA. As expected, higher fields result in more alignment and thus higher mobility. The

accurate dimensions of the monodisperse gold rods were determined by TEM (the averaged diameter and length of 38 mobility selected rods at peak voltage is $d_r = 17.1 \text{ nm}$ and length $L_r = 263 \text{ nm}$; with 4% uncertainty). Using our theory, Equation (2), both the diameter and length of the rods can be extracted directly from the experimental measured mobility in Figure 7. The

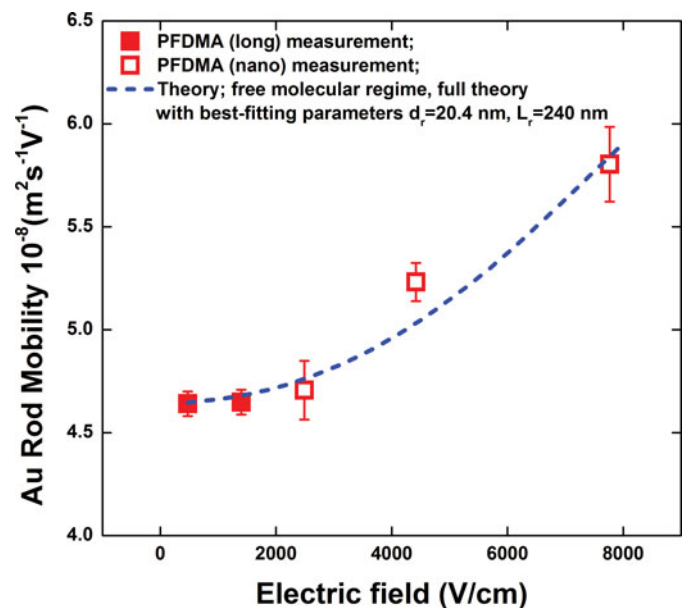


FIG. 7. Experimentally measured mobility for gold rods at various applied fields, where the dimensions of the gold rods were determined by TEM as diameter $d_r = 17.1 \text{ nm}$ and length $L_r = 263 \text{ nm}$. Blue dotted line: full theory for rod with nonlinear least-squares best-fitting parameters, $d_r = 20.4 \pm 0.8 \text{ nm}$ and $L_r = 240 \pm 25 \text{ nm}$. (Color figure available online.)

actual implementation of a nonlinear least square fit to Equation (2) was greatly simplified using the slender rod approximation for the values of polarizability, i.e., Equation (5). A nonlinear least-squares computer procedure (Wolfram Mathematica 8.0; FindFit [parameters] for $5 < d_r < 50$, $5 < L_r/d_r < 50$) was used to fit Equation (2) with the K_{\perp} and K_{\parallel} given in Equations (3a) and (3b)) and the $\langle \cos^2 \theta \rangle$ given in Equations (4) and (5) to the mobility data in Figure 7. From this curve-fitting procedure, the best values of the two parameters, d_r and L_r , were obtained as $d_r = 20.4 \pm 0.8$ nm and $L_r = 240 \pm 25$ nm, which is consistent with the TEM-measured rod dimensions, of $d_r = 17.1$ nm and $L_r = 263$ nm. The rod diameter of the fitting result is off by $\sim 16\%$ compared with the TEM analysis, while the rod length is underestimated by $\sim 9\%$. Possible reasons for this discrepancy are the day-to-day DMA measurement variation, the accuracy of the free molecular expression for this size of gold rod, and the uncertainties of the TEM analysis. Unfortunately, a small uncertainty in mobility is magnified when converted to the nanorod dimension. The best-fitting parameters obtained in this work are based on measurements over five days. The theoretical curve using the full theory with best-fitting parameters, $d_r = 20.4$ nm and $L_r = 240$ nm, is shown as the blue dotted curve in Figure 7. The slender rod approximation based on Equation (5) (which is not shown in the figure) is very close to the full theory and the two theoretical curves are basically overlapped with each other

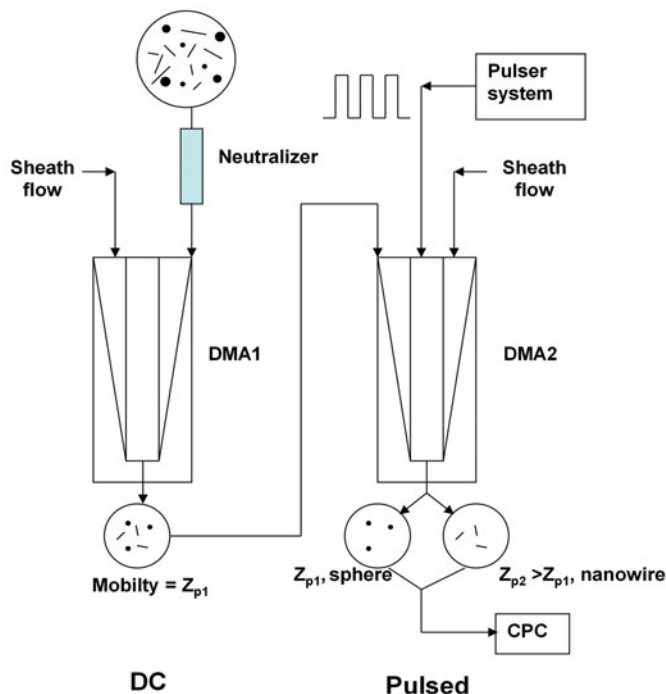


FIG. 8. Measurement system with the first DMA used to select monomobility particles and the pulsed DMA to separate spheres from nanowires and to measure the dimensions of the nanowires. (Color figure available online.)

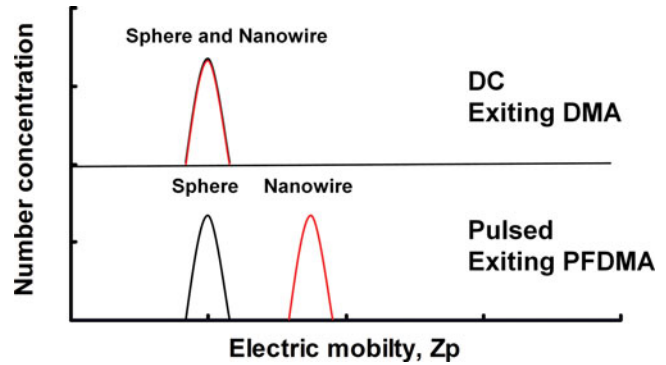


FIG. 9. Schematic illustration of the mobility distribution of particles exiting the DMA-PFDMA system. (Color figure available online.)

(the maximum deviation of the mobility within the plot range between the two theories is 0.23%).

4.4. The Potential of PFDMA for Particle Separation Based on Their Shapes

The effect of particle alignment under electric field, which when implemented with the simplicity of the PFDMA, can be used to separate particles based on their shapes. Two different shape particles having the same mobility size under one value of electric field would show a different mobility size under a different field strength. The evaluation of this approach employs a DMA in series with a PFDMA as shown in Figure 8. Conceptually, if we have a polydisperse distribution of spheres and nanrods entering the first DMA, which is operating at a low-enough field that the particle's orientation is nearly random, then exiting the first DMA is a mixture of nanowires with fixed length and diameter, (nanowires at inlet assumed to have the same diameter), and a fixed diameter of spheres. The alignment effect caused by the second DMA operating in a pulsed mode results in the separation of the nanowires at a lower detection voltage than the spheres. The mobility distributions of the particles exiting the first and second DMA are schematically shown in Figure 9.

5. CONCLUSION

We demonstrate the development and implementation of a pulsed-field DMA to extract nonspherical shape parameters. By using pulsed fields that can orient nonspherical particles, a systematic change in mobility can be obtained, relative to an equivalent sphere. From this orientation effect, particle shapes can be deduced (Li et al. 2012). The instrument was validated with PSL spheres with precisely known size, and gold rods with their dimensions determined by TEM. As a demonstration of potential application, we show how to determine both length and diameter for rod-like particles. The generic approach can be used to obtain dynamic shape factors or other multivariate dimensional information (e.g., length and diameter).

REFERENCES

- Alkilany, A. M., Thompson, L. B., Boulos, S. P., Sisco, P. N., and Murphy, C. J. (2012). Gold Nanorods: Their Potential for Photothermal Therapeutics and Drug Delivery, Tempered by the Complexity of Their Biological Interactions. *Adv. Drug Deliv. Rev.*, 64:190–199.
- Allen, M. D., and Raabe, O. G. (1985). Slip Correction Measurements of Spherical Solid Aerosol-Particles in an Improved Millikan Apparatus. *Aerosol Sci. Technol.*, 4:269–286.
- Cheng, M. T., Xie, G. W., Yang, M., and Shaw, D. T. (1991). Experimental Characterization of Chain-Aggregate Aerosol by Electrooptic Scattering. *Aerosol Sci. Technol.*, 14:74–81.
- Colbeck, I., Atkinson, B., and Johar, Y. (1997). The Morphology and Optical Properties of Soot Produced by Different Fuels. *J. Aerosol Sci.*, 28:715–723.
- Dahneke, B. E. (1973). Slip Correction Factors for Nonspherical Bodies—II Free Molecule Flow. *J. Aerosol Sci.*, 4:147–161.
- Flagan, R. C. (2008). Differential Mobility Analysis of Aerosols: A Tutorial. *Kona Powder Part J.* 26:254–268.
- Guha, S., Li, M., Tarlov, M. J., and Zachariah, M. R. (2012). Electrospray Differential Mobility Analysis of Bionanoparticles. *Trends Biotechnol.*, 30:291–300.
- Kim, S. H., Mulholland, G. W., and Zachariah, M. R. (2007). Understanding Ion-Mobility and Transport Properties of Aerosol Nanowires. *J. Aerosol Sci.*, 38:823–842.
- Kousaka, Y., Endo, Y., Ichitsubo, H., and Alonso, M. (1996). Orientation-Specific Dynamic Shape Factors for Doublets and Triplets of Spheres in the Transition Regime. *Aerosol Sci. Technol.*, 24:36–44.
- Li, M. (2012). Quantifying Particle Properties from Ion-Mobility Measurements, Chemical Physics Program, Dissertation, University of Maryland, College Park. Available online at: <http://hdl.handle.net/1903/13627>.
- Li, M., Guha, S., Zangmeister, R., Tarlov, M. J. and Zachariah, M. R. (2011a). Quantification and Compensation of Nonspecific Analyte Aggregation in Electrospray Sampling. *Aerosol Sci. Technol.* 45:849–860.
- Li, M., Guha, S., Zangmeister, R., Tarlov, M. J., and Zachariah, M. R. (2011b). Method for Determining the Absolute Number Concentration of Nanoparticles from Electrospray Sources. *Langmuir*, 27:14732–14739.
- Li, M., Mulholland, G. W., and Zachariah, M. R. (2012). The Effect of Orientation on the Mobility and Dynamic Shape Factor of Charged Axially Symmetric Particles in an Electric Field. *Aerosol Sci. Technol.*, 46:1035–1044.
- Li, M., Mulholland, G. W., and Zachariah, M. R. (2014). Rotational Diffusion Coefficient (or Rotational Mobility) of a Nanorod in the Free-Molecular Regime. *Aerosol Sci. Technol.* (in review).
- Li, M., You, R., Mulholland, G. W., and Zachariah, M. R. (2013). Evaluating the Mobility of Nanorods in Electric Fields. *Aerosol Sci. Technol.*, 47:1101–1107.
- Ni, W., Kou, X., Yang, Z., and Wang, J. F. (2008). Tailoring Longitudinal Surface Plasmon Wavelengths, Scattering and Absorption Cross Sections of Gold Nanorods. *ACS Nano.*, 2:677–686.
- Schmid, G., and Chi, L. F. (1998). Metal Clusters and Colloids. *Adv. Mater.*, 10:515–526.
- Song, D. K., Lenggoro, I. W., Hayashi, Y., Okuyama, K., and Kim, S. S. (2005). Changes in the Shape and Mobility of Colloidal Gold Nanorods with Electrospray and Differential Mobility Analyzer Methods. *Langmuir*, 21:10375–10382.
- Weiss, R. E., Kapustin, V. N., and Hobbs, P. V. (1992). Chain-Aggregate Aerosols in Smoke from the Kuwait Oil Fires. *J. Geophys. Res.: Atmos.* 97:14527–14531.
- Zelenyuk, A., and Imre, D. (2007). On the Effect of Particle Alignment in the DMA. *Aerosol Sci. Technol.*, 41:112–124.